Precision Inverse Modeling of Highway Pavements Based on Standardized Alignment

Ruifeng Ma, Qing Zhu, Xuming Ge, Xin Jia, Han Hu, *Member, IEEE*, and Tao Liu

***Abstract*—Reconstruction and expansion, as well as asset management, of highways necessitate the development of a current and highly precise 3D pavement model. Current inverse modeling methods with point clouds are laborious, time-consuming, and limited in precision. This article introduces an alternative framework for parametric inverse procedural modeling of highway pavement with standardized alignments seamlessly integrated with off-the-shelf modeling software. It comprises three key steps. (1) *Extraction of highway pavement boundaries and lane markings:* Initially, we combine grid-based and model-driven methods, followed by line structure-based clustering, to accurately generate road centerlines and layouts. (2) *Road centerline generation:* The centerline, derived from lane markings, informs highway alignments and parameters based on geometric characteristics such as curvature and slope. We utilize cost functions to facilitate this process. (3) *Novel inverse procedural assembly:* This innovative step integrates off-the-shelf modeling software. This approach involves extracting vector lines from point clouds and applying constraints at pivotal points on highway pavement cross-sections. Our focus is on refined component-level modeling, allowing for the assembly of diverse highway elements. This method significantly reduces human intervention and achieves high precision. In tests on two highway datasets from Sichuan Province, China, our method achieved excellent results. It attained an average correctness of 98.63% and completeness of 99.66% within a 10 cm error margin. A comparison with the intersection point method indicated minimal errors, with maximum values below 1.2%. The resultant 3D highway pavement model is modular and highly accurate at the centimeter level.**

***Index Terms*—Geometric design standards, highway alignments, inverse procedural modeling, mobile laser scanners (MLS) point clouds.**

I. Introduction

RECENT advancements in smart highway construction emphasize the importance of building information modeling (BIM) in transportation infrastructure. BIM offers crucial benefits, such as improved 3D visualization and integrated information, which are vital throughout the highway construction lifecycle [1], [2]. Highway 3D modeling provides refined geometric information for BIM, serving as a foundation for applying BIM in the highway infrastructure domain. The generated model acts as a carrier for the 3D solid composition structure, attributes, and semantic relationships of components, facilitating areas such as highway reconstruction and expansion, as well as intelligent management of highway assets [3]. However, managing increasing project complexities challenges model updates. To address this issue, remote sensing, especially laser scanning, is widely used in highway maintenance, construction assessment, and asset management, boosting efficiency and precision [4]. Mobile laser scanners (MLS) are cost-effective tools for capturing detailed 3D scenes, surpassing aerial (ALS), and terrestrial laser scanners (TLS) in highway layout extraction and 3D modeling [5].

The automated, efficient, and precise transformation of 3D point clouds into pavement models is crucial for the overall quality of 3D highway models. In the field of highway engineering, standardized alignment refers to a series of parametric curve representation of the centerline of a road's strip-shaped entity surface in 3D space, which conforms to specific design standards and contains some geometric attributes such as curvature, gradient, and superelevation. Thus, it is imperative to ensure that 3D highway models are in compliance with these design standards. While creating 3D models of highway from design blueprints typically aligns well with these standards, the task of modeling existing highways often presents challenges. Utilizing inverse procedural modeling techniques from the domain of computer graphics, this methodology collects point clouds of the existing highway scene to inversely reconstruct parametric curve elements that adhere to highway standard. This process guarantees the effectiveness and precision of the inverse modeling.

Current highway pavement modeling methods still rely heavily on manual work and lack full automation and the efficiency of BIM technology. Achieving detailed modeling in complex highway environments requires a more efficient approach that meets alignment standards and improves automation. Our research emphasizes the precision of component-level modeling on highways. Integrating highway elements such as edges, lanes, and reservations significantly enhances the usability of 3D highway models in transportation applications such as reconstruction and expansion.

Manuscript received 20 January 2024; revised 28 March 2024 and 24 April 2024; accepted 10 May 2024. Date of publication 23 May 2024; date of current version 14 June 2024. This work was supported in part by the National Natural Science Foundation of China under Grant 42230102, in part by the Sichuan Science and Technology Fund for Distinguished Young Scholars under Grant 22JCQN0110, and in part by the National Natural Science Foundation of China under Project 42071437 and Project 62006199. *(Corresponding author: Xuming Ge.)*

Ruifeng Ma, Qing Zhu, Xin Jia, and Tao Liu are with the Faculty of Geomatics, Lanzhou Jiaotong University, Lanzhou 730070, China (e-mail: 1320068@stu.lzjtu.edu.cn; zhuqing@swjtu.edu.cn; 1320066@stu.lzjtu.edu.cn; liutao@lzjtu.edu.cn).

Xuming Ge and Han Hu are with the Faculty of Geosciences and Engineering, Southwest Jiaotong University, Chengdu 611756, China (e-mail: xuming.ge@swjtu.edu.cn; han.hu@swjtu.edu.cn).

Digital Object Identifier 10.1109/JSTARS.2024.3404458

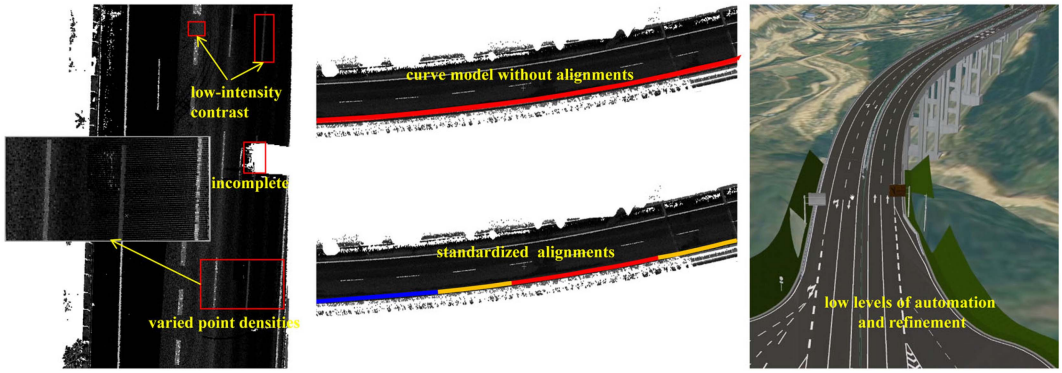

Fig. 1. Some challenges in extracting highway alignment and 3D modeling from MLS point clouds are illustrated. (a) Some challenges for road marking and boundary extraction. (b) Standardized alignments or curve model. (c) Manual highway pavement 3D model and low level of refinement.

The primary challenges in extracting highway alignment and 3D modeling from MLS point clouds include the following aspects.

First, automatically extracting standardized alignment, which includes a series of parametric curves, poses a significant challenge. Traditionally, identifying finer, connected features such as road boundaries and markings has been difficult. This difficulty arises from the low-intensity contrast between road markings and surrounding pavement, incomplete road markings or boundaries, and varied point densities [6], as shown in Fig. 1(a). Moreover, the automated extraction of precise standardized alignments, not only modeling curves, represents a crucial advancement in broadening its extensive applicability, as shown in Fig. 1(b).

Second, the current methods for highway pavement modeling are characterized by low levels of automation, being time-consuming and labor-intensive, and the detail of the pavement modeling is insufficient, not reaching the level of component-based modeling. The constructed models are primarily focused on applications in visualization, where their accuracy is constrained, as shown in Fig. 1(c).

To address these key challenges, we propose a framework for parametric inverse procedural refined modeling of highway pavement. This approach utilizes standardized alignment and the modeling application programming interface (API) provided by a 3D modeling solution. The main contributions of this study are as follows.

1) The development of an inverse procedural refined modeling framework for highway pavement from MLS point clouds that conforms to standardized alignment.
2) The achievement of high-accuracy extraction of standardized alignment elements and their parameters, leveraging spline modeling of points, geometric characteristics, and a comprehensive cost function.
3) A novel inverse procedural assembly method for refined modeling is presented. Based on standardized alignment, this method completes inverse modeling by extracting vector lines representing diverse components from point clouds and applying constraints at key points on highway pavement cross-sections.

II. Related Works

In this section, we provide a concise overview of relevant literature, including topics such as extracting road boundaries and markings from point cloud data, as well as highway alignment extraction and 3D modeling.

A. Road Boundary and Marking Extraction From MLS Point Clouds

Road boundary extraction: Several methods are available for obtaining road boundaries, mainly focusing on curb extraction by assessing local point distributions. These methods fall into two categories [7]: 3D point-based and scanline-based methods. The 3D point-based approach uses unorganized points as input and applies techniques such as smooth surfaces or polynomials combined with local pattern detection to efficiently extract road edges [8], [9], [10]. Although it is efficient and mitigates accuracy losses, it relies on smooth surfaces or polynomials, potentially omitting certain road boundary details, especially in irregular scenarios such as highways with uneven curbs and grass strips [11]. Conversely, scanline-based methods offer advantages in terms of lower computational demands and the ability to extract accurate road boundaries irrespective of the MLS system speed [7], [12], [13]. Recently, supervoxel-based methods have gained attention for their adaptability in handling various road scenarios [14], [15].

Road marking extraction: Highway markings play a vital role in digitizing highway data and aiding in extracting alignments and 3D modeling. There are two main groups of methods for road marking extraction: Bottom-up and top-down methods [16]. Bottom-up methods start with low-level features such as intensity thresholds to differentiate road markings from their surroundings [17], [18], [19]. While effective, they are sensitive to data quality. In contrast, top-down methods use predefined geometric models, which rely less on data quality but take more time [20], [21], [22]. Recent advancements in deep learning have led to researchers using neural networks for high-level feature identification and classification of road markings, improving accuracy [6], [23], [24], [25]. However, challenges such as handling large-scale environments, sample imbalances, and extreme

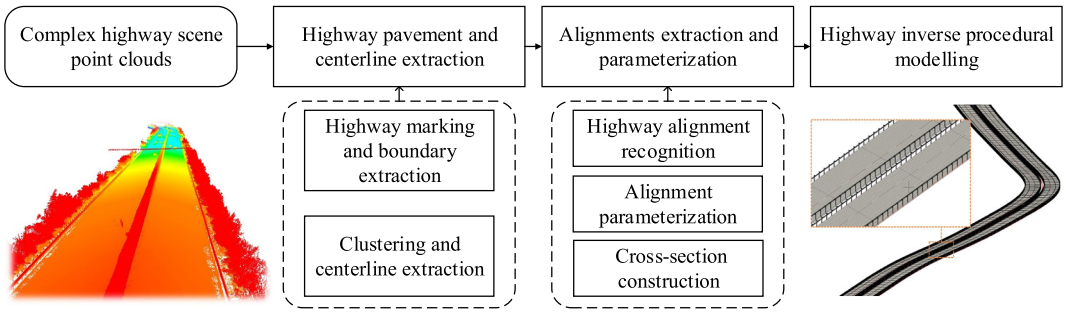

Fig. 2. Overall workflow of the proposed method.

scale variations among categories remain to be addressed in further research.

B. Highway Alignment Extraction and 3D Modeling

Highway alignment: Highway alignment, as per design specifications, involves horizontal components such as straight lines, circular arcs, and clothoids and vertical components such as straight lines and parabolas [26]. Prior to the extensive application of MLS data, trajectory data from mobile mapping system (MMS) was the primary source for characterizing the geometric properties of highways [27], [28]. Typically, the centerline was estimated from trajectory data collected during two traversals of the MMS in opposite directions. However, the road geometry reconstructed in this manner is heavily dependent on the trajectory of the MMS and is constrained by the point density in the trajectory data, which in turn affects the accuracy of alignment extraction. The advent of MLS data has markedly improved both accuracy and point density [29]. Methods for extracting highway alignments from MLS data fall into two categories: curve fitting-based and specification-based methods. Curve fitting-based methods use curves such as splines for digital representation, offering straightforward mathematical modeling and visualization but often deviating from design specifications, limiting their use in construction quality assessment [30], [31], [32]. Specification-based approaches strictly follow design specifications, providing comprehensive outputs suitable for tasks such as construction inspection and 3D modeling [33], [34], [35], [36]. These approaches use geometric-driven [37], [38], [39] and RANSAC model-driven strategies [40], [41]. Geometric-driven methods rely on data quality and often need manual intervention for accuracy. In contrast, RANSAC model-driven approaches, though noise-resistant, struggle with setting internal thresholds, impacting their stability.

Highway 3D modeling: Highway 3D modeling holds significant importance, and several methods have been introduced. In [42], an automated method was introduced for the 3D modeling of intricate highway interchanges by integrating laser scanning data with 2D topographic maps. In [4], a semiautomated approach that processes MLS point clouds to produce an industry foundation class (IFC)-compliant file was developed, which models both the alignment and the centerline of each lane on a highway. In [40], highway pavement boundaries and lane markings were identified first, then highway alignments were extracted from ALS data, and finally, 3D highway models were reconstructed constrained by the identified alignments. Nonetheless, these methods have not yet achieved component-level 3D modeling of highways, limiting their broader application. Recently, a method [43] for creating digital twins of highways using map data was proposed, focusing on key highway components. However, precision limitations in data could affect modeling accuracy, raising concerns about data availability in specific areas.

In this study, we propose a semiautomatic framework for parametric inverse procedural modeling of highways utilizing standardized alignment and the modeling API offered by a 3D modeling solution. Fig. 2 presents the flowchart of the proposed approach, followed by detailed stage descriptions.

III. Highways Standardized Alignment

As previously stated, our research, informed by road engineering expertise, focuses on delineating highway alignments along the road's centerline. Fig. 3 illustrates the extraction process. Initially, the road centerline is extracted from highway markings. Subsequently, the horizontal and vertical alignments, as well as the road's cross-section, are derived in accordance with geometric design standards. These elements are parameterized according to the mathematical alignment model.

A. Road Centerline Extraction

Highway scenes contain complex MLS point clouds. The 3D curvature of a road is typically captured by the centerline near the central reserve. The focus begins with identifying the highway pavement and then extracting and grouping highway markings and road boundaries. Eventually, the virtual road centerline is derived backward from the highway markings.

1) Highway Marking and Boundary Extraction: We sorted ground and nonground points in the MLS data using the surface filter method [44]. Then, we identified highway pavement points among the ground points based on flat surfaces, lower intensity than nearby elements, and the presence of road curbs or sloped shoulders.

First, we establish a horizontal, square-shaped grid by dividing the ground points. Then, for each partitioned grid, compute the 3D covariance matrix and perform eigenvalue decomposition

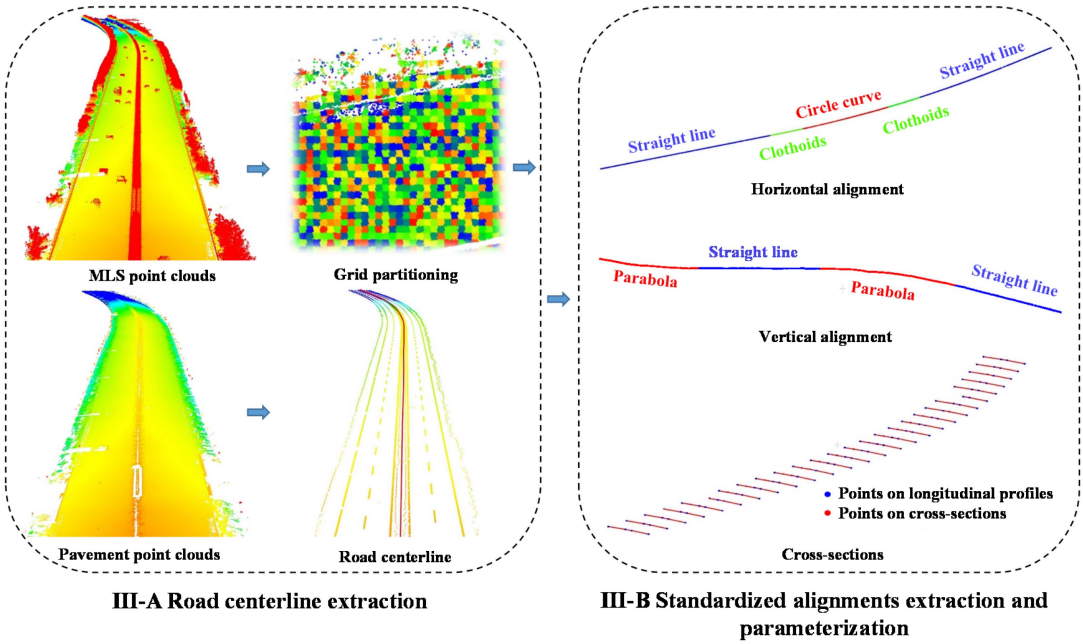

Fig. 3. Highway standardized alignment recognition.

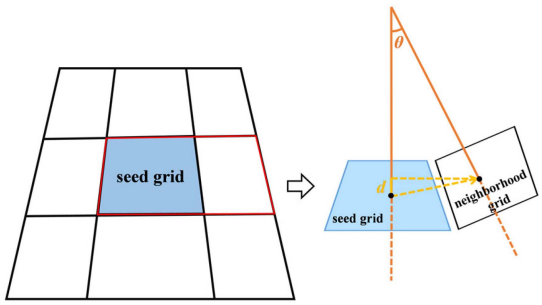

Fig. 4. Growing procedure within the eight neighbors of seed gird. (a) Eight neighbors of seed gird. (b) Angle between normal vectors and the projected displacement as growth conditions.

based on principal component analysis (PCA). Set a threshold for the minimum eigenvalue to retain flat grids as smooth highway pavement grids, using the minimum eigenvalue as the normal vector, and define the plane passing through the grid point cloud's centroid as the local fitting plane for that grid. Using the smoothed grid as the seeds, apply two specified criteria as growth conditions within an eight-neighborhood when $\theta < \theta_\zeta$ and $\mathrm{d} < \mathrm{d}_\lambda$, where θ represents the angle between normal vectors, and d denotes the projected displacement (Fig. 4). The largest area resulting from region growth is selected as the initial area for the highway pavement. Finally, refine the pavement point cloud based on the initial highway pavement area. The method involves calculating, for each point in the grids surrounding the initial pavement area, the distance to the adjacent local fitting plane and the intensity difference between the point and the adjacent grid point cloud. After computing for all qualifying points, output the refined pavement point cloud. Fig. 5 displays the results of the pavement point clouds extracted from the MLS raw highway point clouds.

Upon obtaining highway pavement point clouds, we hypothesized that highway markings are included in this subset. We then utilized this subset to identify highway markings, which are vital for road inventory management, lane division, and depicting the longitudinal profile of the pavement structure. Despite challenges such as noise, diverse terrain, and variations in marking wear and occlusion, the methodology [22] successfully automates the extraction of highway markings. It addresses discontinuities in solid line markings within complex highway scenes by employing a prior knowledge of marking design rules and edge-based matching model that leverages the standard geometric template and radiometric appearance of highway markings.

Next, we extracted boundary points from the highway pavement to delineate highways. By employing the 2D α-shaped algorithm [45], we achieved this effectively.

Fig. 6 illustrates the results of highway markings and boundaries extracted from pavement point clouds. These highway markings and boundaries form control lines that are essential for refined depicting the pavement layout. Prior to this, it is critical to cluster these control lines and calculate a virtual road centerline, which plays a significant role in the extraction of highway alignments.

2) Line Structure-Based Clustering and Centerline Extraction: Using conventional methods to cluster highway pavement control lines from point clouds faces challenges due to the nonlinear nature of highways. Their frequent horizontal curvature, instead of uniform straightness, makes it difficult to rely solely on distance and density criteria.

We developed an iterative least squares line clustering method based on the spatial relationships of points. The process initially utilizes an oriented bounding box to partition control lines using a threshold (σ) of 50 m and attain precise linear approximations. Following partitioning, each subset of points undergoes line

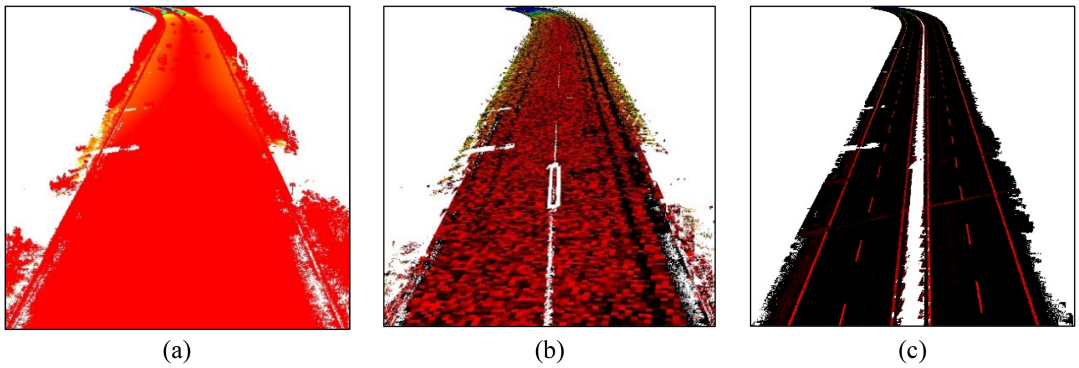

Fig. 5. Highway pavement extraction. (a) Raw highway point clouds. (b) Partitioning of point clouds into grids. (c) Pavement point clouds.

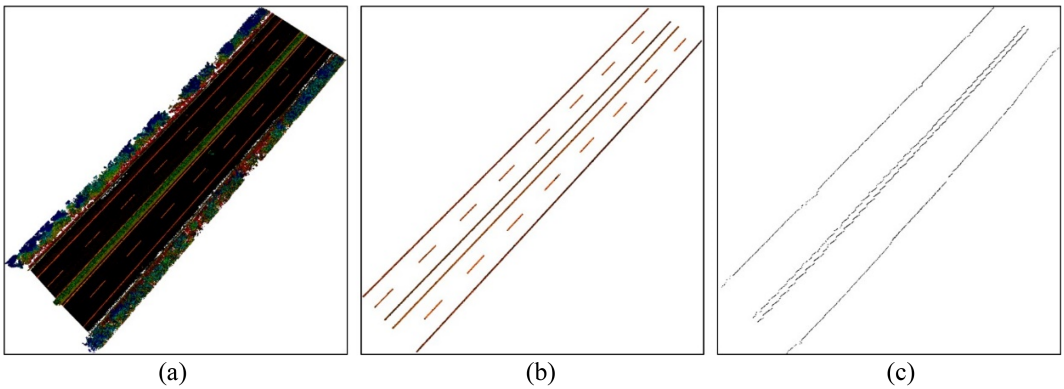

Fig. 6. Highway marking and boundary extraction. (a) Raw highway point clouds. (b) Lane marking points. (c) Highway pavement boundary points.

structure-based clustering, as detailed in the pseudocode of Algorithm 1. Subsequent to these operations, the distinct clusters within these subsets are merged. Fig. 7 displays the intermediate and final clustering results on a subset of points, differentiating them with various colors.

Upon gathering highway marking and boundary data, we generate a virtual road centerline to account for the absence of the actual centerline in the collected point clouds. This includes extracting the centerline from the two nearest highway markings near the central reserve. Our algorithm downsamples these markings every meter, identifies the closest point for pairing by iterating through the denser marking, and computes the average coordinate value, defining it as the central point's coordinates.

B. Standardized Alignment Extraction and Parameterization

After obtaining the highway centerline point clouds, we identified standardized alignments, mathematical models and parameter ranges in Table I, as delineated in [34]. Equation (1) unifies the horizontal and vertical alignment at specific locations. Our recognition process segmented centerline points based on geometric principles governing various curve elements. Horizontal alignment was determined based on its relationship with curvature, whereas vertical alignment was identified through its correlation with slope. Fig. 8(a) and (b) present graphical illustrations that depict these geometric relationships clearly.

$$\begin{cases} \mathrm{x}\ (\mathrm{m}) = \mathrm{x}_0\ + \int_0^{\mathrm{m}} \cos\left(\varphi + \kappa \mathrm{t} + \frac{1}{2}\psi \mathrm{t}^2\right) dt \\ \mathrm{y}\ (\mathrm{m}) = \mathrm{y}_0\ + \int_0^{\mathrm{m}} \sin\left(\varphi + \kappa \mathrm{t} + \frac{1}{2}\psi \mathrm{t}^2\right) dt \\ \mathrm{z}\ (\mathrm{m}) = \mathrm{z}_0\ + \ \xi m + \frac{1}{2}\eta \mathrm{m}^2 \end{cases} \tag{1}$$

where x_0, y_0, and z_0 represent the start location, the variable m is the cumulative length of all sequence points ranging from (x_0, y_0, z_0) to $(x(m), y(m), z(m))$ projected in the X-Y plane, φ is the horizontal azimuth, κ is the horizontal curvature, ψ is the change rate of the horizontal curvature, ξ is the vertical slope, and η is the vertical curvature.

1) Alignment Extraction and Parameterization: Sampling points using B-spline curves. In road centerline extraction, B-spline curves alleviate outliers and fluctuations in 3D data. These methods reduce errors in calculating parameters such as the curvature and slope from discrete points. The process includes resampling, knot generation, basis function computation, control point updates, and sampling. This creates a smooth continuous curve, yielding discrete data points.

Initially, we computed distances between 3D centerline points $\mathrm{P}_{\text{center}} = \{\mathrm{p}_1, \mathrm{p}_2, \ldots, \mathrm{p}_{\mathrm{n_p}}\}$. The normalized spacing to each point was based on cumulative distances. Then, we conducted

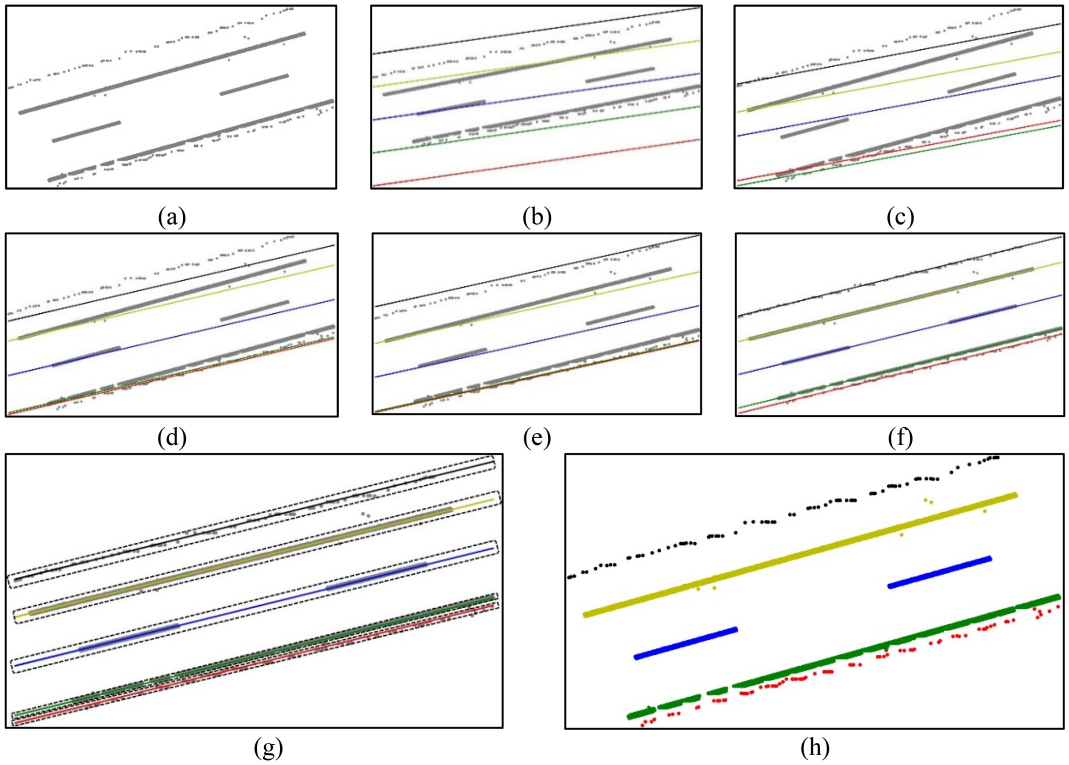

Fig. 7. Clustering process using line structure. (a) Highway marking and boundary point clouds in a block. (b) Initial line structure. (c) First iteration result using least squares fitting. (d)–(f) Clustering line structure after progressive multiple iterations. (g) Final line clustering structure. (h) Results of line structure-based clustering presented using different colors for the highway markings and boundaries.

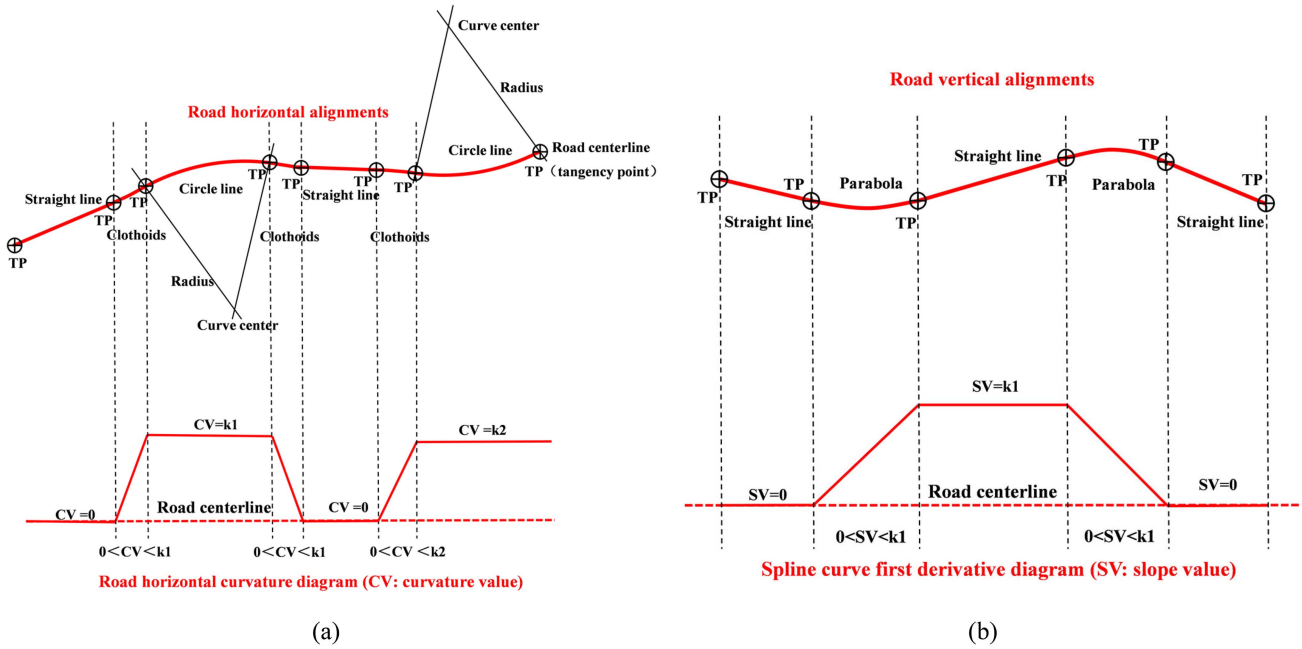

Fig. 8. Graphical diagram of road alignment geometry. (a) Geometric relationship between horizontal alignment and curvature. (b) Geometric relationship between vertical alignment and slope.

Algorithm 1: Line structure-based clustering.

Input: Point Cloud = {P} ∈ highway marking and boundary point clouds.

Output: Cluster point cloud objects ***K***= *{K_1, K_2, K_3 … K_n}*, K_n represent a clustering object, n is the number of clusters, in our cases n = 5.

Initialization of slope *m* and intercept *c*.

1. A = create a matrix with x-coordinates and ones
2. m, c = compute linear regression on A and y-coordinates
3. initialize intercepts for five lines: c_1, c_2, c_3, c_4, c_5

Iterate for clustering and updating lines.

4. ***For i = 0 to 10***
5. calculate y-distances to each line
6. classify points into clusters based on distances
7. $k_1, \ldots, k_5$ stores the logical index used for clustering, respectively
8. ***For n = 0 to 5***
9. create a submatrix A_{K_5} using x-coordinates and ones from points in Cluster K_5
10. compute linear regression for Cluster K_5: m_5, c_5
11. compute average slope m = (m_1+m_2+m_3+m_4+m_5)

Divide into 5 clusters.

12. cluster according to updating $k_1, \ldots, k_5$ to retrieve points for finishing cluster objects K = *{K_1, K_2, K_3, K_4, K_5}*

spacing resampling according to the following equation:

$$r(\mathrm{i}) = \begin{cases} 0 & \text{if } i = 0 \\ 1 & \text{if } i = \mathrm{n_{cp}} - 1 \\ \mathrm{s\,(j)} & \text{if } c\,(\mathrm{j}) = w\,(i) \\ \mathrm{s\,(j)} + (\mathrm{s\,(j+1)} - \mathrm{s\,(j)}) \cdot \frac{\mathrm{w(i)-c(j)}}{\mathrm{c(j+1)-c(j)}} & \text{if } \mathrm{c\,(j)} < w\,(i) \end{cases} \tag{2}$$

where $\mathrm{r(i)}$ denotes the linear interpolation results for the resampling spacing, with $\mathrm{i} \in (0, \mathrm{n_{cp}} - 1)$, where $\mathrm{n_{cp}}$ is the number of control points. $\mathrm{s(j)}$ and $\mathrm{s(j+1)}$ represent consecutive elements in the original spacing vector **s**. $\mathrm{c(j)}$ and $\mathrm{c(j+1)}$ are consecutive elements in the vector **c**, which represents the normalized positions of the original spacing values over the range [0, 1]. The j is an index that iterates over the elements of the original spacing vector **s** and the current sample points vector **c**, with $\mathrm{j} \in [1, \mathrm{n_p} - 2]$, where $\mathrm{n_p}$ represent the number of original samples. Moreover, $\mathrm{w(i)}$ signifies the expected sampling, which is also within the range of [0, 1].

Next, we established the knot vector KV using resampling spacing $\mathrm{rs(i)}$, $\mathrm{n_{cp}}$ control points, and the order k. This vector is critical in determining the spline curves within intervals. Then, we computed the basis function coefficients using the Cox-de-Boor formula [refer to (3)], which is essential for B-spline curve interpolation. For a $\mathrm{k} = 3$ B-spline curve with a knot vector $\mathbf{t} = \{\mathrm{t_0}, \ldots, \mathrm{t_{n+k}}\}$, the recursive formulation of the B-spline basis function $\mathrm{B_{i,k}(t)}$ is

$$\mathrm{B_{i,0}\ (t)} = \begin{cases} 1 & \text{if } \mathrm{t_i} \le t \le \mathrm{t_{i+1}} \\ 0 & \text{otherwise} \end{cases}$$

$$\mathrm{B_{i,k}\,(t)} = \frac{\mathrm{t - t_i}}{\mathrm{t_{i+k} - t_i}}\,\mathrm{B_{i,k-1}\,(t)} + \frac{\mathrm{t_{i+k+1} - t}}{\mathrm{t_{i+k+1} - t_{i+1}}}\mathrm{B_{i+1,k-1}\,(t)} \tag{3}$$

where $\mathrm{t_i}$ to $\mathrm{t_{i+k}}$ define the nonzero interval of the basis function $\mathrm{B_{i,k}(x)}$, which is the B-spline basis function of degree k defined over the vector **t** at the parameter value x. Subsequently, the control points are updated using centerline points and basis coefficients, improving the curve. New centerline points are then derived from the refined B-spline curve, matching the original input points. Fig. 9 shows 3D views of these centerline point samplings via B-splines.

Segmentation centerline point for curve element recognition: We segment curve elements using the curvature of sampled centerline points, aligning with road geometry principles. To estimate curvature, we apply the least squares circle fitting method locally, yet initial measurements may contain noise and outliers, especially in straight segments. To address this issue, we use the Hampel filter to identify and replace outliers in the curvature values. This filter operates with a sliding window, computing the median and median absolute deviation (MAD) to detect outliers. If an observation deviates by more than t standard deviations from the median, it is replaced. The adjustable parameters of the filter are h (window half-width) and t (standard deviations for outlier identification). Equations (4)–(7) illustrate this filtering process.

$$\mathrm{W_i^h} = \{\mathrm{k_{i-h}}, \ldots, \mathrm{k_i}, \ldots, \mathrm{k_{i+h}}\} \tag{4}$$

$$\mathrm{m_i} = \mathrm{median}\,\{\mathrm{k_{i-h}}, \ldots, \mathrm{k_i}, \ldots, \mathrm{k_{i+h}}\} \tag{5}$$

$$\mathrm{S_i} = \lambda \times \mathrm{median_{j\in[-h,\,h]}}\,\{\mathrm{k_{i-j}} - \mathrm{m_i}\},\ (\lambda = 1.4826) \tag{6}$$

$$\mathrm{f\,(k)} = \begin{cases} \mathrm{k_i} & |\mathrm{k_i} - \mathrm{m_i}| \le t\mathrm{S_i} \\ \mathrm{m_i} & |\mathrm{k_i} - \mathrm{m_i}| > t\mathrm{S_i} \end{cases} \tag{7}$$

where h, a positive integer, serves as the window half-width. The standard median filter, $\mathrm{M_i} = \{\mathrm{m_1}, \ldots, \mathrm{m_i}, \ldots, \mathrm{m_n}\}$, is derived by calculating the median of the moving data window $\mathrm{W_i^h}$. $\mathrm{S_i}$ denotes the MAD scale estimate, and setting $\lambda = 1.4826$ renders the MAD scale estimate an unbiased estimator of the standard deviation for Gaussian data. Furthermore, we employ curvature criteria to refine curve segmentation, as shown in Fig. 8(a). Initially, a threshold of 0.03 was used to identify straight-line points that met the minimum radius standards for roads without superelevation [46]. To detect points on circular curves, we identify local curvature maxima using a sliding window technique. This helps mark multiple local maxima, distinguishing points related to distinct curves. Points not meeting these criteria are categorized as clothoid points.

In road engineering, the highway's longitudinal profile is the vertical intersection line between the centerline and pavement projected along the road's length. Using the B-spline curve for 3D points optimizes sample points in the elevation direction. We determined elevations at 1-meter intervals along the centerline, calculating slopes for these values. To classify the

TABLE I
MATHEMATICAL MODEL AND PARAMETER RANGES FOR CURVE ELEMENTS

Alignment	Curve elements	Mathematical model	Parameter ranges
Horizontal alignment	*Straight line*	$\begin{cases} x(m) = x_0 + mcos\varphi \\ y(m) = x_0 + msin\varphi \end{cases}$	$\varphi \in [0,2\pi)$, $\kappa \in [-0.05,0.05]$, $\psi \in [-0.0025,0.0025]$
	Circle line	$\begin{cases} x(m) = x_0 + (sin(\varphi + \kappa m) - sin\varphi)/\kappa \\ y(m) = y_0 - (cos(\varphi + \kappa m) - cos\varphi)/\kappa \end{cases}$	
	Clothoids	$\begin{cases} x(m) = x_0 + \int_0^m cos\left(\varphi + \kappa t + \frac{1}{2}\psi t^2\right) dt \\ y(m) = y_0 + \int_0^m sin\left(\varphi + \kappa t + \frac{1}{2}\psi t^2\right) dt \end{cases}$	
Vertical alignment	*Straight line*	$z(m) = z_0 + m\xi$	
	Parabola	$z(m) = z_0 + m\xi + \frac{1}{2}\eta t^2$	$\xi \in [-0.2,0.2]$, $\eta \in [-0.01,0.01]$

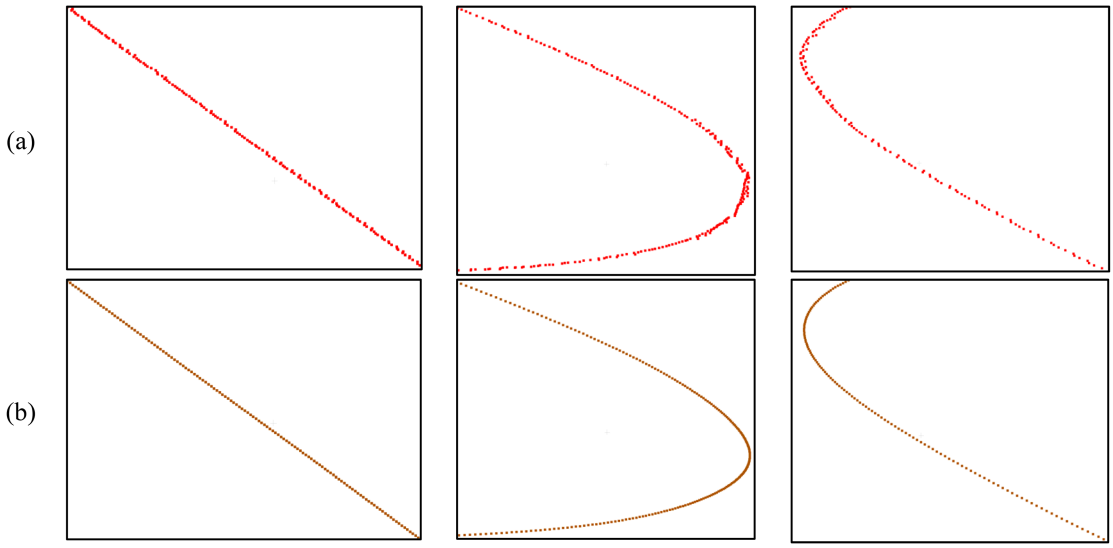

Fig. 9. Enlarged local 3D views of 3D centerline point sampling results using B-splines in some typical parts. (a) Original centerline points above. (b) Sampling centerline points below.

profile, we analyzed the slope relationships with the vertical curve characteristics. By computing the derivative of the filtered slopes, segments with a consistent zero derivative are identified as straight lines, while the rest are recognized as parabolic segments.

Highway alignment parameterization: To parameterize highway alignment, we refine the progressive approach [40] using an energy model minimization technique. This method optimizes the parameters shaping the curve by iteratively adjusting them to closely match the observed data. The aim is to minimize differences between predicted and actual data points, enhancing the accuracy of the modeled curve in representing the highway. The optimization focuses on three aspects: Reducing discrepancies between the data and model points, aligning their directions for each curve segment, and minimizing differences in the calculated curvature values. These steps collectively ensure smoother transitions between curve segments.

The process of parameterization can be illustrated using horizontal alignment as an example. Equations (8) and (9) are utilized to fit the horizontal position of the curve elements and to compute the direction at a specific point on the curve, respectively. In this context, m represents the parameter of the current center point, while P, representing the parameters on a curve element, is defined as $\mathrm{P} = \{\varphi, \kappa, \psi\}$.

$$\begin{cases} \mathrm{x}\ (\mathrm{m}, \mathrm{P}) = \mathrm{x}_0\ + \int_0^{\mathrm{m}} \cos\left(\varphi + \kappa \mathrm{t} + \frac{1}{2}\psi \mathrm{t}^2\right) dt \\ \mathrm{y}\ (\mathrm{m}, \mathrm{P}) = \mathrm{y}_0\ + \int_0^{\mathrm{m}} \sin\left(\varphi + \kappa \mathrm{t} + \frac{1}{2}\psi \mathrm{t}^2\right) dt \end{cases} \tag{8}$$

$$\mathrm{dir}\,(\mathrm{m}, \mathrm{P})\ = \varphi + \kappa \mathrm{m} + \frac{1}{2}\psi \mathrm{m}^2. \tag{9}$$

The optimization method can be described in (10)–(13), where E represents the energy model and consists of three terms $\mathrm{E}_{\mathrm{distance}}$, $\mathrm{E}_{\mathrm{dirction}}$ and $\mathrm{E}_{\mathrm{curvature}}$, to minimize them as a cost function of optimization

$$\mathrm{E}\ = \mathrm{E}_{\mathrm{distance}}\ + \mathrm{E}_{\mathrm{dirction}} + \mathrm{E}_{\mathrm{curvature}} \tag{10}$$

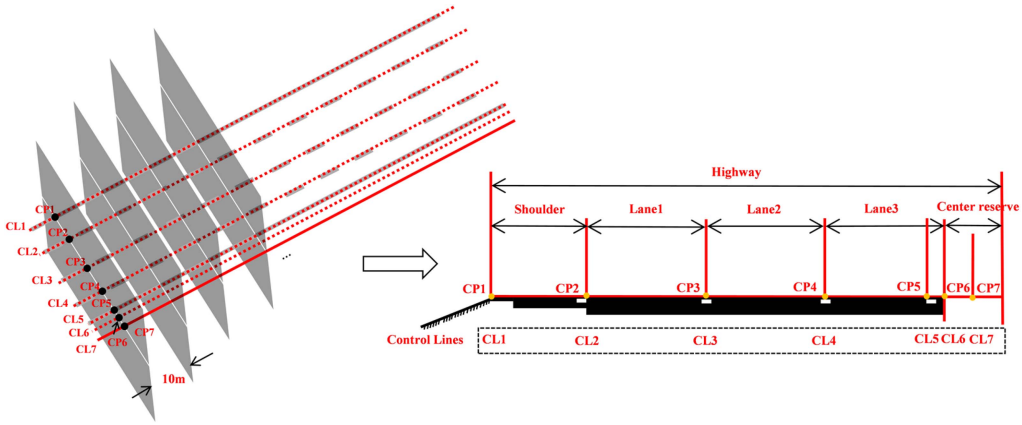

Fig. 10. Highway cross-section: the left panel shows the process of constructing the cross-section, and the right panel shows the slice and its corresponding control lines.

$$\mathrm{E_{distance}} = \sum_{i=1}^{n} \sum_{j=1}^{s} \{[x_{i,j} - x(m_{i,j}, P_i)]^2 + \{[y_{i,j} - y(m_{i,j}, P_i]^2\} \tag{11}$$

$$\mathrm{E_{dirction}} = (\mathrm{Mdir}_0^{i-1} - \varphi^i)^2 + \left(\mathrm{Mdir}_1^{i-1} - \varphi^i + k^i m_i + \frac{1}{2}\psi^i {m_i}^2\right)^2 \tag{12}$$

$$\mathrm{E_{curvature}} = \left|k^i + m_i \psi^i - k^{i+1}\right| \tag{13}$$

where n denotes the number of segmented curve elements and s is the number of points on each individual segment. The parameters Mdir_0^{i-1} and Mdir_1^{i-1} represent the principal directions at the starting and ending points of the previous segment, respectively. m_i represents the accumulated distance of the ith alignment element, and ψ^i represents the change in curvature. This principal direction is computed using PCA within a certain neighborhood of points.

Upon constructing the cost function, we implement Ceres Solver,[1] an open-source C++ library designed for modeling and solving nonlinear least squares problems. This solver is applied to iteratively determine the parameters of each curve element, progressively alternating adjustments between m and P.

2) Cross-Section Construction: Cross-sections offer a 2D representation of roads perpendicular to their longitudinal axis. Following Section III-A methods with control lines and a centerline, we create highway cross-sections that capture the geometric layout of the line. We start by downsampling key control lines for lanes and boundaries at one-meter intervals. B-spline interpolation refines these lines, providing crucial points at one-meter intervals for lane marking and digital modeling. Next, we generate cross-sectional planes every 10 meters perpendicular to the centerlines. Intersection points of control lines in each plane create a 2D model of highway cross-sections. These control points are defined by the mathematical model from the previous step. Fig. 10 illustrates this construction, highlighting distinct control points (e.g., CP1, CP2) constrained by their control lines (e.g., CL1, CL2).

IV. Inverse Modeling Combining 3D Modeling Solution API

We automated highway inverse modeling using alignments, control lines defining lanes and road boundaries, and commercial modeling APIs. Our method converts highway alignments into compatible formats for modeling APIs, guiding the highway's 3D trajectory. We strategically position key points along the highway alignment using control lines, creating detailed 3D models directly from point clouds.

This approach constructs modular 3D highway models comprising lanes, shoulders, and more, allowing selective attribute queries. Integration with digital Earth frameworks requires a high-precision digital elevation model (DEM) derived from point cloud data and the filtering of nonground points to construct the DEM's triangular mesh.

V. Experiments and Analysis

A. Dataset Description

We applied our method to create 3D models using two datasets sourced from highway point clouds in Sichuan Province, China, obtained using the iScan Mobile Measuring System (MMS).[2] Fig. 11(a) shows the iScan MMS process, while Fig. 11(b) illustrates its panorama camera and laser scanner. Table II details MMS performance indices. The scanner's $-30°$ orientation [seen in Fig. 11(a)] optimizes transverse coverage at high speeds. Trajectory data were collected using global navigation satellite systems and an inertial measurement unit on the MMS. Fig. 11(c) displays the collected point clouds, color-coded by intensity. Dataset I covers 5.7 km long single-direction point clouds with circular curves of various radii. Dataset II comprises a 4.8 km bidirectional road, with the first half following an overall subgrade design and the latter half using a separate type (as

[1] [Online]. Available: http://ceres-solver.org/

[2] [Online]. Available: https://www.zhdgps.com/detail/car_portable-Hi Scan-C

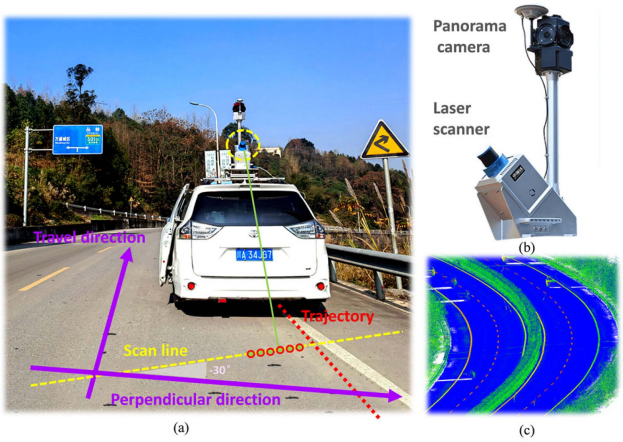

Fig. 11. (a) Scanner configuration of the iScan MMS. (b) Enlarged view of the panorama and laser scanner. (c) Highway scene point cloud colored by intensity values.

TABLE II
PERFORMANCE INDEX OF THE MLS SYSTEM

Parameters	Scan point frequency	Scanning frequency	Measuring distance	Field of view	Distance measurement accuracy
Performance index	≥50 million points/second	≥200 Hz	300 m	≥360°	≤6 mm∼40 m

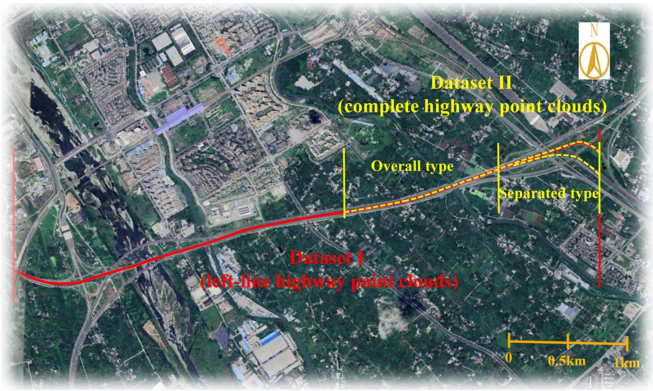

Fig. 12. Overview of the two datasets. Dataset I only contains left-line highway point clouds. Dataset II contains complete highway point clouds and consists of the overall type and separated type.

shown in Fig. 12). Table III provides a quantitative analysis of both datasets. Our programs, developed in C++ using the open-source Point Cloud Library (PCL),[3] ran experiments on a standard computer with 64 GB of RAM and an AMD Ryzen 7 5800X 8-Core Processor operating at 3.80 GHz.

[3][Online]. Available: https://pointclouds.org/

TABLE III
QUANTITATIVE DESCRIPTIONS OF DATASETS I AND II

Datasets	Road length(km)	Data collection integrity
I	5.7	Only left-line highway point clouds
II	4.8	Complete highway point clouds

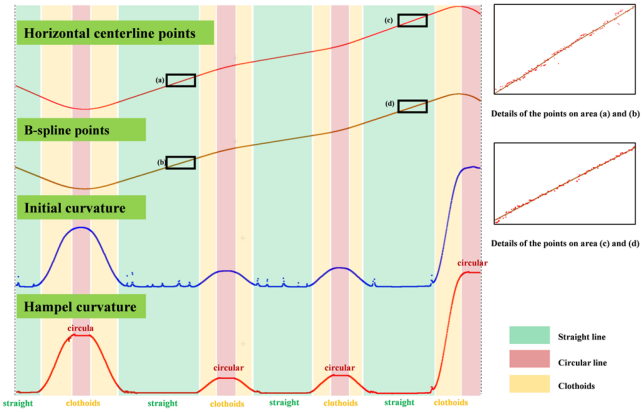

Fig. 13. Horizontal alignment recognition using curvature.

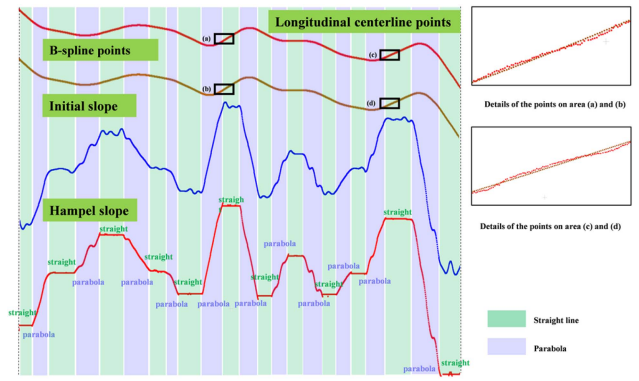

Fig. 14. Vertical alignment recognition using slope.

B. Alignment Recognition Results

1) Qualitative Evaluation: Utilizing the methods outlined in Section III and their respective parameter configurations, distinct curve elements were extracted and identified from the two datasets. Figs. 13 and 14 illustrate the extraction process and results for the highway alignments in Dataset I. This includes intermediate results for horizontal alignment, encompassing B-spline fitting, sampling, initial curvature computation, and filtering, as well as for vertical alignment, which involves B-spline fitting, sampling, initial slope computation, and slope filtering.

The rectangular boxes (a), (b), (c), and (d) in Fig. 13 demonstrate that after B-spline fitting, the curves show enhanced smoothness, and significantly reduced outliers, data fluctuations, and gaps caused by occlusion. Preliminary analysis of the initial curvature plot indicates that Dataset 1 contains four

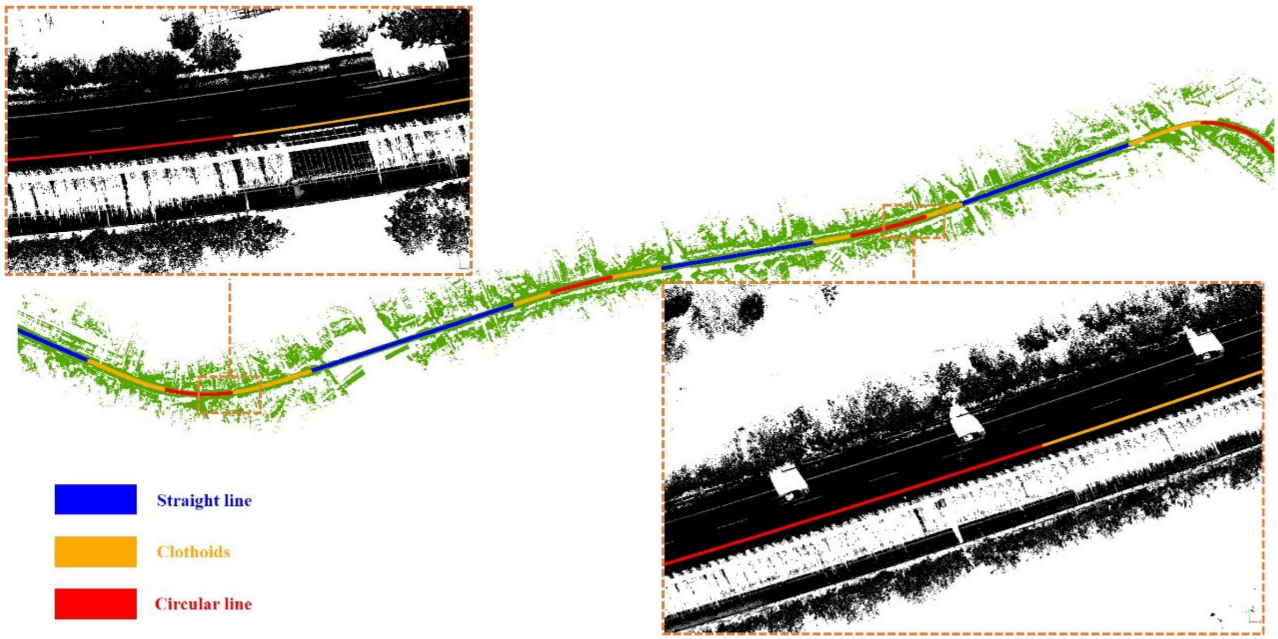

Fig. 15. Highway alignments extracted results Dataset I. The details in the box depict the overlay of the 3D highway alignments and the original point cloud.

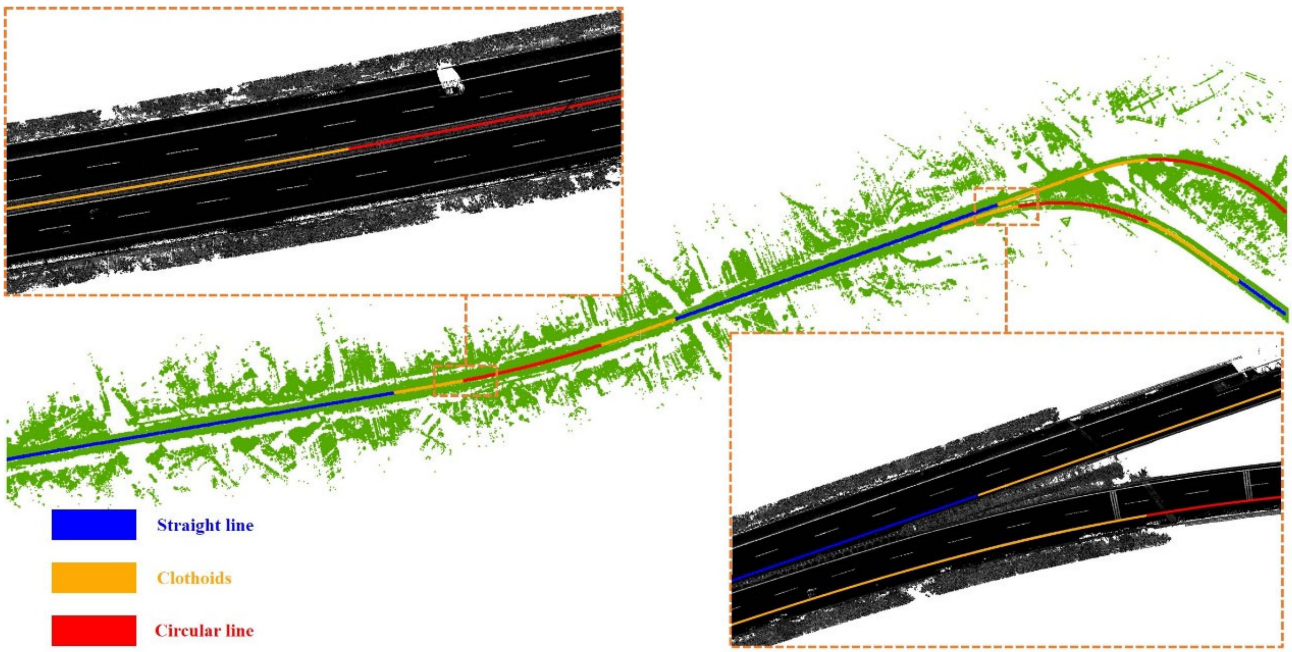

Fig. 16. Highway alignments extracted results Dataset II. The details in the box depict the overlay of the 3D highway alignments and the original point cloud.

circular curves, seven transitional curves, and four straight-line segments. Notably, extensive circular curves seamlessly integrate with straight-line segments through transitional curves, complying with highway design standards. However, challenges arise in accurately locating the boundary points of different curve elements due to varying noise levels and oversmoothing of curvature values. Applying Hampel filtering improves the delineation of boundary features for different curve elements markedly and reduces curvature noise substantially. This enhancement aids in the precise identification of boundary points in the proposed method. Fig. 14 demonstrated that despite Dataset I's location in a flat terrain with minimal vertical variations, our methodology effectively identifies various vertical elements, including 12 lines and 11 parabolas.

Figs. 15 and 16 illustrate the overlay of 3D highway alignments extracted from Datasets I and II onto the original point

TABLE IV
QUANTITATIVE EVALUATION OF HIGHWAY ALIGNMENTS ON DATASETS I AND II

Buffer size	Dataset I		Dataset II	
	Correctness (%)	Completeness (%)	Correctness (%)	Completeness (%)
5 cm	96.65	98.32	97.14	95.29
10 cm	98.63	99.65	98.62	99.67

clouds, including detailed views of specific sections. These extracted alignments are fully 3D and precisely delineate highway trends. After parameterization, the method enables the extraction of parameters adhering to highway specifications for segmented curve elements. This process allows for a comparison between the derived parameters and forward design deviations, providing a reverse-engineering approach that aids in assessing the quality of highway construction.

2) Quantitative Evaluation: Upon extracting the alignments, we employed the buffer-overlay-statistics method [47] for a quantitative evaluation of the results. This method yields reliable measures of geometric accuracy for line datasets, evaluating aspects such as spatial accuracy, completeness, oscillation, and bias relative to a comparative dataset. In our experiments, the extracted highway alignments are denoted as H_a, and the reference data, H_r, are manually extracted from the MLS point cloud. Initially, we establish specific buffer zones, labeled H_aB_i and H_rB_i. To analyze varying levels of uncertainty and sensitivity to different scales, we implemented various buffer sizes, such as B_i(i.e., 5 and 10 cm). Next, we conduct overlay analyses for H_aB_i and H_rB_i, corresponding to H_a and H_r, respectively. Finally, we compute statistics to evaluate the correctness and completeness, employing the formulas in (14) and (15).

The sum of $\mathrm{H_a}$ inside $\mathrm{H_rB_i}$ represents the total length of the extracted alignments from $\mathrm{H_a}$ within $\mathrm{H_rB_i}$, which is then compared to the overall length of the lines in $\mathrm{H_a}$. Similarly, $\mathrm{H_r}$ inside $\mathrm{H_aB_i}$ is the aggregate length of the reference alignments from $\mathrm{H_r}$ within $\mathrm{H_aB_i}$, compared to the total line length in $\mathrm{H_r}$. Table IV presents the quantitative evaluation results for Datasets I and II. Consequently, our proposed method achieves an average correctness of 98.63% and an average completeness of 99.66% at the 10 cm level reference buffers for extracted alignments across the two datasets. Given these evaluation outcomes, we endorse a method that demonstrates utility in various fields, especially in generating high-definition (HD) maps at the lane level, assessing road completion, and evaluating road safety.

$$\text{correctness} = \frac{\text{length}(\mathrm{H_a\ inside\ H_rB_i})}{\text{length}(\mathrm{H_a})} \tag{14}$$

$$\text{completeness} = \frac{\text{length}(\mathrm{H_r\ inside\ H_aB_i})}{\text{length}(\mathrm{H_r})}. \tag{15}$$

3) Comparative Analysis: Furthermore, we conducted a comparative analysis of highway alignments in Dataset I, comparing the results obtained using the intersecting point method from Bentley OpenRoads Designer[4] and our proposed methods, as detailed in Table V. Considering the frequent unavailability or absence of design parameters for existing roads, verifying the accuracy of the proposed methods poses a significant challenge. We propose that the results from the intersecting point method be considered as the ground truth for inverse highway alignment extraction.

Table V presents a comparison of the alignments obtained via the intersecting point method and those obtained via the proposed method. $\mathrm{D_{cumulative}}$ represents the cumulative distance of the alignments. UTM X and UTM Y denote the coordinates of the singular points of the alignments. $\mathrm{E_R}$ shows the errors in the alignment results of the proposed method relative to those of the intersecting point method. Equation (16) defines this error as the ratio of the discrepancy between the values from the proposed method and the ground truth (values from the intersecting point method) to the ground truth. Initially, the series of alignments extracted by the proposed method aligns perfectly with those obtained through the intersecting point method. In terms of $\mathrm{E_R}$, the proposed method demonstrates relatively minor relative errors, all below 1.2%. For instance, the largest deviation observed is between the radius of the intersection point method (2, 955.51 m) and the radius determined by the proposed method (2, 988.42 m), which occurs in the alignment at a cumulative distance of 2, 417.66.

$$\mathrm{E_R} = (\mathrm{R_P} - \mathrm{R_I}) / \mathrm{R_I} \tag{16}$$

where $\mathrm{E_R}$ is the relative error of the radius, $\mathrm{R_I}$ is the radius obtained by the intersecting point method, and $\mathrm{R_P}$ is the radius obtained by the proposed method.

C. Inverse Procedural Modeling Results

Owing to our prior acquisition of highway alignments and their parameters, cross-sections, and control lines for various highway components, we effectively implemented highway inverse procedural modeling, as proposed in Section IV. We selected specific highway sections from Dataset II to demonstrate various control lines and key points on road cross-sections, as depicted in Fig. 17. The importation of extracted alignments and control lines, in addition to the configuration of corresponding cross-sections, enables the automated generation of a 3D highway pavement model through an inverse assembly process, as depicted in Fig. 18.

The methodology for obtaining these data, along with the quantitative evaluation of control lines and key points, is comprehensively detailed in Table VI. In Table VI, "HBE" and "HME" denote highway boundary extraction and highway marking extraction, respectively. The symbols ζ_θ and λ_d refer to the highway pavement extraction parameters outlined in

[4][Online]. Available: https://www.bentley.com/software/openroads-designer/

TABLE V
COMPARISON OF ALIGNMENTS ACCORDING TO THE INTERSECTING POINT METHOD AND THE PROPOSED METHOD

$D_{cumulative}$	Intersecting point method				Proposed method				E_R
	UTM X	UTM Y	Alignment	Radius	UTM X	UTM Y	Alignment	Radius	
0.00	367,924.84	3,426,168.45	Straight	_	367,921.63	3,426,169.82	Straight	_	
334.46	368,235.42	3,426,035.54	Clothoid	_	368,232.26	3,426,036.89	Clothoid	_	
691.66	368,559.58	3,425,913.97	Curve	803.96	368,566 74	3,425,912.33	Curve	811.17	0.89 %
976.42	368,852.48	3,425,900.60	Clothoid	_	368,849.29	3,425,900.15	Clothoid	_	
1,331.02	369,184.74	3,425,991.45	Straight	_	369,190.89	342,599,345	Straight	_	
2,249.59	370,070.85	3,426,278.75	Clothoid	_	370,067.76	3,426,277.74	Clothoid	_	
2,417.66	370,230.96	3,426,329.75	Curve	2,955.51	370,227.87	3,426,328.83	Curve	2,988.42	1.11 %
2,683.65	370,488.90	3,426,394.27	Clothoid	_	370,485.75	3,426,393.63	Clothoid	_	
2,894.85	370,696.92	3,426,431.05	Straight	_	370,693.72	3,426,430.52	Straight	_	
3,568.95	371,367.93	3,426,545.04	Clothoid	_	371,361.51	3,426,543.95	Clothoid	_	
3,733.95	371,517.72	3,426,570.90	Curve	2,540.35	371,520.89	3,426,571.50	Curve	2,537.49	0.77 %
4,059.24	371,841.76	3,426,654.91	Clothoid	_	371,838.69	3,426,653.90	Clothoid	_	
4,221.73	372,001.45	3,426,710.37	Straight	_	371,992.22	3,426,707.15	Straight	_	
4,994.44	372,727.36	3,426,965.26	Clothoid	_	372,721.28	3,426,963.09	Clothoid	_	
5,316.94	373,020.04	3,427,052.32	Curve	395.24	373,029.85	3,427,052.94	Curve	397.74	0.63
5,660.71	373,332.34	3,426,936.20	Clothoid	_	373,339.12	3,426,929.12	Clothoid	_	

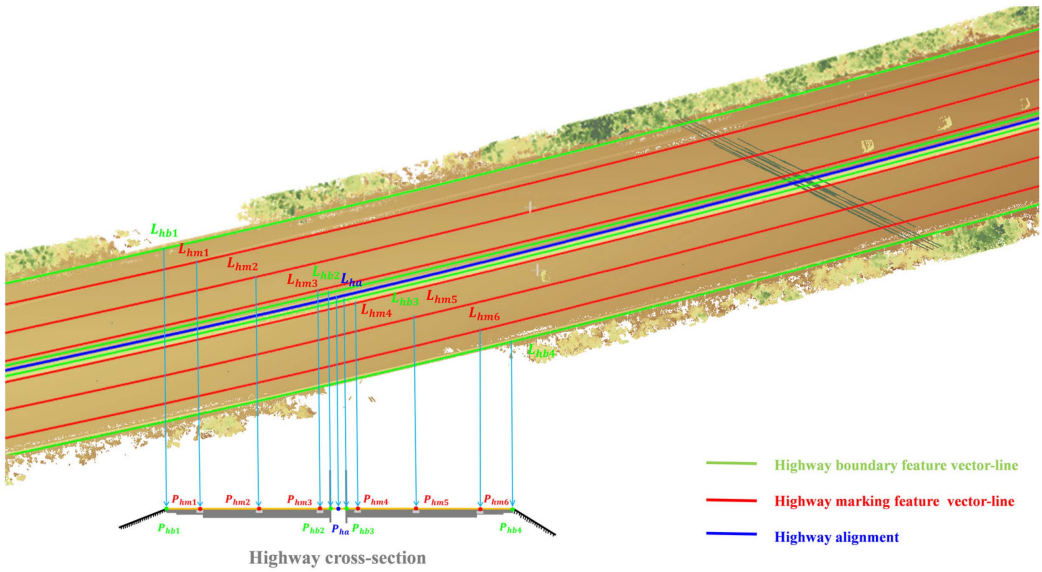

Fig. 17. Constraint feature line and corresponding key points on the highway cross-section.

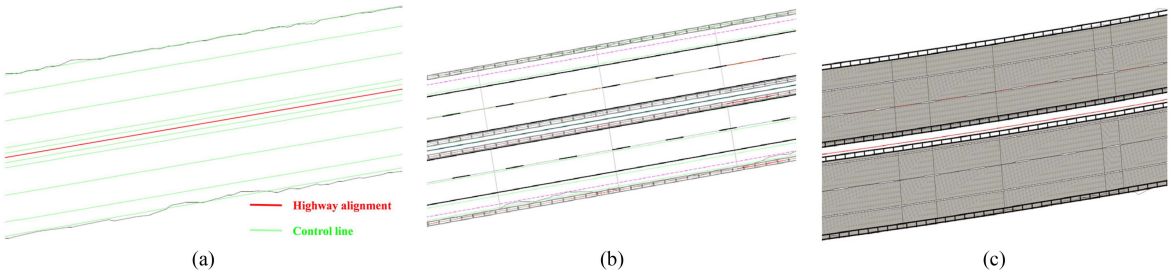

Fig. 18. Inverse assembly process. (a) Highway alignments and control line. (b) Assembling diverse elements. (c) Generating a 3D model of highway pavement.

TABLE VI
PARAMETERS OF THE CONSTRAINT POINTS AND CONTROL LINES AND THEIR EVALUATION

Control lines	Constraint points	Method	ζ_θ	λ_d	φ_1	φ_2	φ_3	RMSE
L_{hb1}	P_{hb1}	HBE & fit	10	0.05	_	_	_	0.0864
L_{hm1}	P_{hm1}	HME & fit	_	_	8	0.6	0.2	0.0283
L_{hm2}	P_{hm2}	HME & fit	_	_	8	0.6	0.2	0.0324
L_{hm3}	P_{hm3}	HME & fit	_	_	8	0.6	0.2	0.0227
L_{hb2}	P_{hb2}	HBE & fit	10	0.05	_	_	_	0.1453
L_{ha}	P_{ha}	Section B	_	_	_	_	_	Section III-B
L_{hb3}	P_{hb3}	HBE & fit	10	0.05	_	_	_	0.1728
L_{hm4}	P_{hm4}	HME & fit	_	_	8	0.6	0.2	0.0284
L_{hm5}	P_{hm5}	HME & fit	_	_	8	0.6	0.2	0.0256
L_{hm6}	P_{hm6}	HME & fit	_	_	8	0.6	0.2	0.0332
L_{hb4}	P_{hb4}	HBE & fit	10	0.05	_	_	_	0.0738

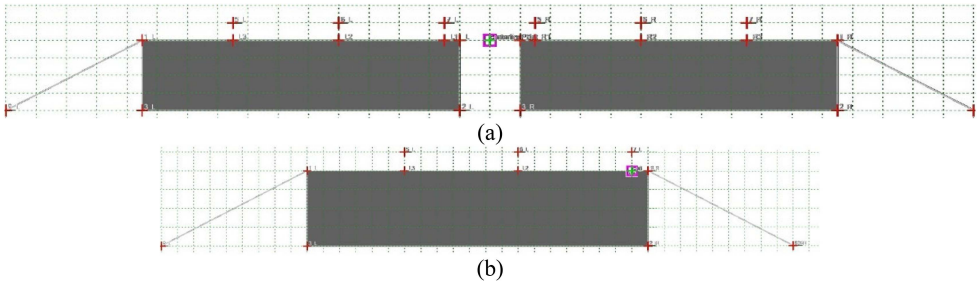

Fig. 19. Two different highway cross-sectional template designs in modeling software. (a) Overall type of highway cross-section. (b) Separated type of highway cross-section (left section).

Section III-A-1). Additionally, φ_1, φ_2 and φ_3 represent parameters of the rule-based extraction of highway markings, conforming to specifications and ensuring robustness and effectiveness, as outlined in [22]. For a single cross-section type, the process involves designing only a highway cross-section template, adding key points, and setting vector control line constraints. However, for transition zone roads that feature multiple cross-section types within a single highway, a segmented approach is necessary for cross-section creation, with additional interactions required to manage transition regions between cross-sections. Furthermore, for road segments that comprise both overall and separated cross-sections (as illustrated in Dataset II), the procedure begins with identifying the centerlines for overall and separate sections independently. Fig. 19 showcases two different highway cross-section template designs in modeling software. Typically, centerlines in an overall cross-section are located near the central reserve, whereas in a separated cross-section, they originate from the center lane or side lanes. Modeling baselines are then established based on these distinct centerlines, followed by the application of a procedural reverse-engineering process. Fig. 20 presents the overall modeling results for Dataset II, and Fig. 21 depicts the modeling details of a real 3D highway model at various locations.

D. Discussion, Comparison, and Analysis

The experimental results clearly demonstrate that our method accurately extracts precise highway alignments, control lines, and key points from point clouds, enabling detailed, refined 3D modeling. This method generates control lines that precisely match key points, which is crucial for assembling detachable,

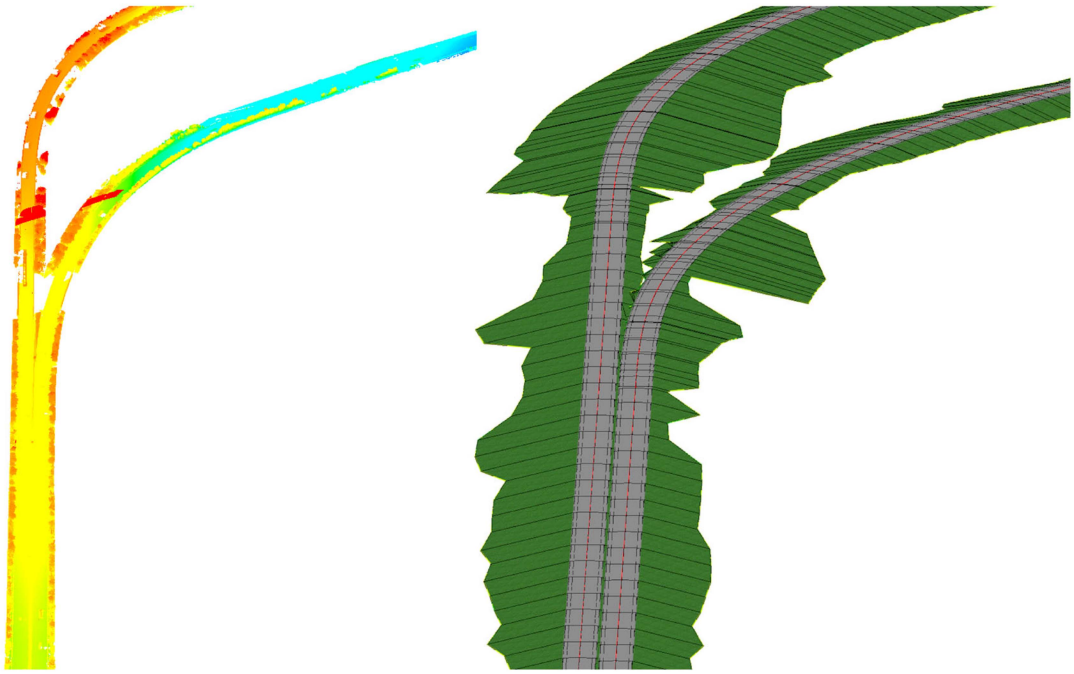

Fig. 20. 3D modeling results of highways with cross-sections of the overall type in dataset II. (a) Point clouds of highway. (b) 3D model of highway.

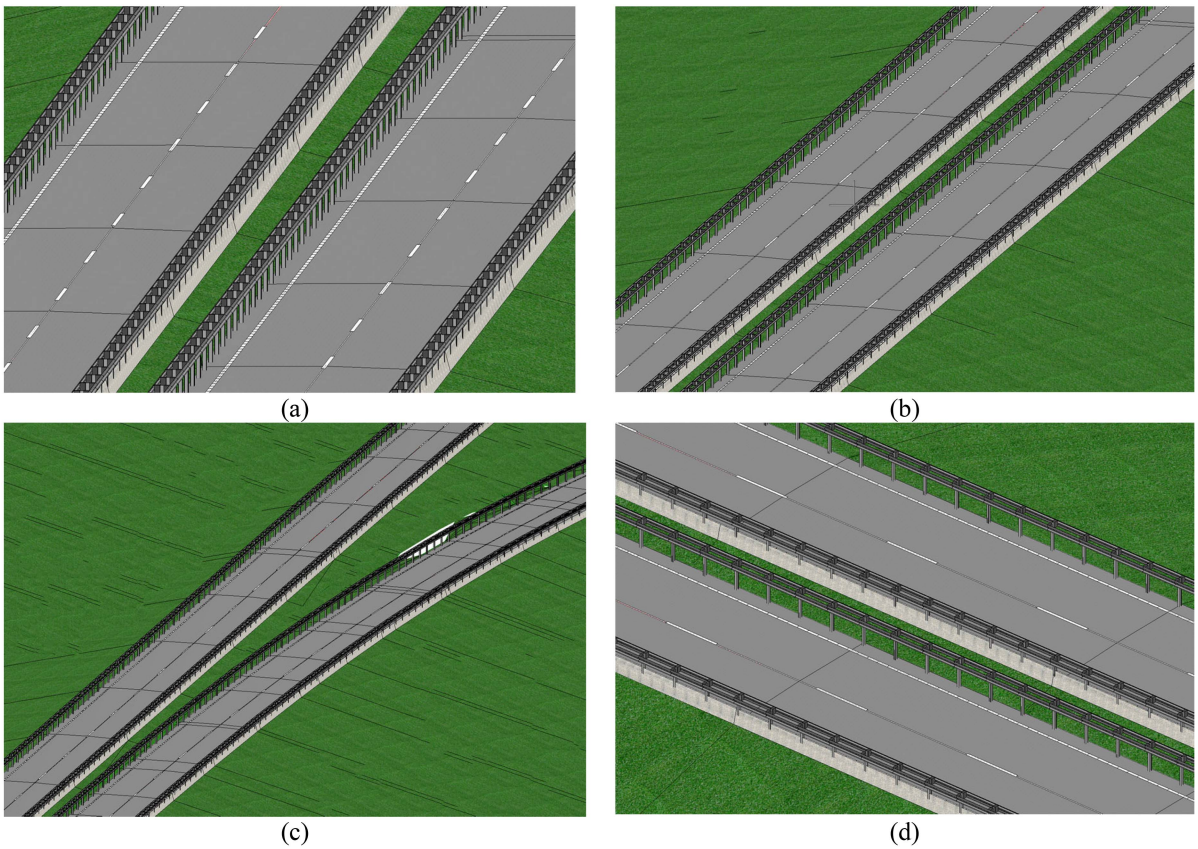

Fig. 21. Modeling details of highway real 3D models at different locations.

real 3D models at the component level. The extracted alignments and parameters meet road engineering standards and have applications in highway reconstruction, HD map generation, and road safety assessments. The refined 3D model integrates seamlessly with BIM+GIS-based applications, allowing for smooth integration with surrounding elements and aiding in creating precise highway digital twins.

The proposed method has practical application potential and has achieved remarkable results. We qualitatively compared the different state-of-the-art methods for converting point clouds to 3D models. Our method stands out in two key aspects: First, it automatically extracts precise 3D highway alignments and parameters from point clouds, integrating seamlessly into 3D modeling APIs; second, it extracts feature lines such as lane markings and road boundaries from point clouds for control lines for refined modeling. Both Zhou's [40] and our method use high-precision point clouds for highway alignments and 3D modeling. However, Zhou's approach focuses on depicting the entire highway surface without providing a detailed representation of the road surface, limiting its application in transportation. In contrast, Jiang's method [43] relies heavily on existing aerial photography and DEM data, posing challenges in terms of precision. Furthermore, within the proposed framework, the extraction of highway alignments and 3D modeling operate independently, enabling effortless integration with widely employed point cloud processing tools that extract road boundaries and markings.

VI. Conclusion

In this study, we presented an effective framework for parametric inverse procedural modeling of highways by merging standardized alignment and refined pavement structures into existing modeling software using MLS point clouds. Our innovative approach involves an automated process for the precise extraction of highway alignments and an inverse procedural assembly method for refined modeling. Our experiments revealed two key findings: (1) Achieved high precision in alignment extraction with 10 cm accuracy, scoring approximately 98.63% for average correctness and 99.66% for average completeness across datasets. Comparative analysis revealed minimal relative errors compared with the intersecting point method, with deviations less than 1.2%. (2) The use of precise alignments and pavement structures enhances 3D highway model refinement and modularity. Our method produces detachable and extensible pavement models, improving BIM quality. While our approach demonstrates strengths, future enhancements could focus on (1) expanding highway components using ALS/TLS point cloud fusion and (2) accelerating the extraction processes for highway markings and boundaries.

References

[1] A. Bradley et al., "BIM for infrastructure: An overall review and constructor perspective," *Automat. Construction*, vol. 71, pp. 139–152, 2016.

[2] V. Vignali et al., "Building information modelling (BIM) application for an existing road infrastructure," *Automat. Construction*, vol. 128, 2021, Art. no. 103752.

[3] Q. Zhu et al., "From real 3D modeling to digital twin modeling," *Acta Geodaetica et Cartographica Sinica*, vol. 51, no. 6, pp. 1040–1049, 2022.

[4] M. Soilán et al., "3D point cloud to BIM: Semi-automated framework to define IFC alignment entities from MLS-acquired LiDAR data of highway roads," *Remote Sens.*, vol. 12, no. 14, 2020, Art. no. 2301.

[5] Q. Zhu et al., "Multiple point clouds data fusion method for 3D city modeling," *Wuhan Daxue Xuebao (Xinxi Kexue Ban)/Geomatics Inf. Sci. Wuhan Univ.*, vol. 43, pp. 1962–1971, 2018.

[6] C. Wen et al., "A deep learning framework for road marking extraction, classification and completion from mobile laser scanning point clouds," *ISPRS J. Photogrammetry Remote Sens.*, vol. 147, pp. 178–192, 2019.

[7] H. Ryohei, H. Date, and S. Kanai, "Extraction of road edges from MLS point clouds using bend angle of scanlines," *Int. Arch. Photogrammetry Remote Sens. Spatial Inf. Sci.*, vol. 43, pp. 1091–1097, 2020.

[8] B. Rodríguez-Cuenca et al., "Morphological operations to extract urban curbs in 3D MLS point clouds," *ISPRS Int. J. Geo-Inf.*, vol. 5, no. 6, 2016, Art. no. 93.

[9] B. Yang et al., "3D local feature BKD to extract road information from mobile laser scanning point clouds," *ISPRS J. Photogrammetry Remote Sens.*, vol. 130, pp. 329–343, 2017.

[10] L. Ma, Y. Li, J. Li, J. M. Junior, W. N. Gonçalves, and M. A. Chapman, "BoundaryNet: Extraction and completion of road boundaries with deep learning using mobile laser scanning point clouds and satellite imagery," *IEEE Trans. Intell. Transp. Syst.*, vol. 23, no. 6, pp. 5638–5654, Jun. 2022.

[11] L. Ma et al., "Mobile laser scanned point-clouds for road object detection and extraction: A review," *Remote Sens.*, vol. 10, no. 10, 2018, Art. no. 1531.

[12] R. Miyazaki, M. Yamamoto, and K. Harada, "Line-based planar structure extraction from a point cloud with an anisotropic distribution," *Int. J. Automat. Technol.*, vol. 11, pp. 657–665, 2017.

[13] K. Ishikawa, D. Kubo, and Y. Amano, "Curb detection and accessibility evaluation from low-density mobile mapping point cloud data," *Int. J. Automat. Technol.*, vol. 12, pp. 376–385, 2018.

[14] D. Zai et al., "3-D road boundary extraction from mobile laser scanning data via supervoxels and graph cuts," *IEEE Trans. Intell. Transp. Syst.*, vol. 19, no. 3, pp. 802–813, Mar. 2018.

[15] X. Mi, B. Yang, Z. Dong, C. Chen, and J. Gu, "Automated 3D road boundary extraction and vectorization using MLS point clouds," *IEEE Trans. Intell. Transp. Syst.*, vol. 23, no. 6, pp. 5287–5297, Jun. 2022.

[16] X. Mi et al., "A two-stage approach for road marking extraction and modeling using MLS point clouds," *ISPRS J. Photogrammetry Remote Sens.*, vol. 180, pp. 255–268, 2021.

[17] J. Jung et al., "Efficient and robust lane marking extraction from mobile lidar point clouds," *ISPRS J. Photogrammetry Remote Sens.*, vol. 147, pp. 1–18, 2019.

[18] L. Yao et al., "Automatic extraction and recognition of road markings based on vehicle laser point cloud," *ISPRS Ann. Photogrammetry Remote Sens. Spatial Inf. Sci.*, vol. 2, pp. 313–319, 2020.

[19] Y. Pan et al., "Automatic road markings extraction, classification and vectorization from mobile laser scanning data," *Int. Arch. Photogrammetry Remote Sens. Spatial Inf. Sci.*, vol. 42, pp. 1089–1096, 2019.

[20] B. Soheilian, N. Paparoditis, and D. Boldo, "3D road marking reconstruction from street-level calibrated stereo pairs," *ISPRS J. Photogrammetry Remote Sens.*, vol. 65, no. 4, pp. 347–359, 2010.

[21] A. Hervieu, B. Soheilian, and M. Brédif, "Road marking extraction using a MODEL&DATA-DRIVEN Rj-Mcmc," *ISPRS Ann. Photogrammetry Remote Sens. Spatial Inf. Sci.*, vol. 2, pp. 47–54, 2015.

[22] R. Ma et al., "Model-driven precise degradation analysis method of highway marking using mobile laser scanning point clouds," *Photogrammetric Eng. Remote Sens.*, vol. 89, no. 4, pp. 245–258, 2023.

[23] M. Chen et al., "A semantic segmentation method for vehicle-borne laser scanning point clouds in motorway scenes," *Photogrammetric Rec.*, vol. 38, pp. 117–194, 2023.

[24] X. Han, Z. Dong, and B. Yang, "A point-based deep learning network for semantic segmentation of MLS point clouds," *ISPRS J. Photogrammetry Remote Sens.*, vol. 175, pp. 199–214, 2021.

[25] L. Ma et al., "Capsule-based networks for road marking extraction and classification from mobile LiDAR point clouds," *IEEE Trans. Intell. Transp. Syst.*, vol. 22, no. 4, pp. 1981–1995, Apr. 2021.

[26] HSDC, "Design specification for highway alignment," CCCC Highway Survey Design Company, Ministry of Transport of the People's Republic of China, 2018.

[27] G. Marinelli et al., "Mobile mapping systems and spatial data collection strategies assessment in the identification of horizontal alignment of highways," *Transp. Res. Part C: Emerg. Technol.*, vol. 79, pp. 257–273, 2017.

[28] H. D. F. Santiago and M. Castro, "A method to identify and classify the vertical alignment of existing roads," *Comput.-Aided Civil Infrastructure Eng.*, vol. 32, pp. 952–963, 2017.

[29] A. Holgado-Barco et al., "Semiautomatic extraction of road horizontal alignment from a mobile LiDAR system," *Comput.-Aided Civil Infrastructure Eng.*, vol. 30, no. 3, pp. 611–613, 2014.
[30] M. Castro et al., "Geometric modelling of highways using global positioning system (GPS) data and spline approximation," *Transp. Res. Part C: Emerg. Technol.*, vol. 14, no. 4, pp. 233–243, 2006.
[31] L. Ma, Y. Li, J. Li, Z. Zhong, and M. A. Chapman, "Generation of horizontally curved driving lines in HD maps using mobile laser scanning point clouds," *IEEE J. Sel. Topics Appl. Earth Observ. Remote Sens.*, vol. 12, no. 5, pp. 1572–1586, May 2019.
[32] F. Jiménez, F. Aparicio, and G. Estrada, "Measurement uncertainty determination and curve-fitting algorithms for development of accurate digital maps for advanced driver assistance systems," *Transp. Res. Part C: Emerg. Technol.*, vol. 17, no. 3, pp. 225–239, 2009.
[33] L. Garach, J. D. Oña, and M. Pasadas, "Mathematical formulation and preliminary testing of a spline approximation algorithm for the extraction of road alignments," *Automat. Construction*, vol. 47, pp. 1–9, 2014.
[34] Z. Zhang, J. Li, Y. Guo, C. Yang, and C. Wang, "3D highway curve reconstruction from mobile laser scanning point clouds," *IEEE Trans. Intell. Transp. Syst.*, vol. 21, no. 11, pp. 4762–4772, Nov. 2020.
[35] G. Marinelli et al., "Mobile mapping systems and spatial data collection strategies assessment in the identification of horizontal alignment of highways," *Transp. Res. Part C: Emerg. Technol.*, vol. 79, pp. 257–273, 2017.
[36] X. Tong, X. Meng, and K. Ding, "Estimating geometric parameters of highways and railways using least-squares adjustment," *Surv. Rev.*, vol. 42, pp. 359–374, 2010.
[37] A. Holgado-Barco et al., "An automated approach to vertical road characterisation using mobile LiDAR systems: Longitudinal profiles and cross-sections," *ISPRS J. Photogrammetry Remote Sens.*, vol. 96, pp. 28–37, 2014.
[38] A. Holgado-Barco et al., "Semiautomatic extraction of road horizontal alignment from a mobile LiDAR system," *Comput.-Aided Civil Infrastructure Eng.*, vol. 30, no. 3, pp. 217–228, 2014.
[39] A. Holgado-Barco, B. Riveiro, and D. Gonzalez-Aguilera, "Automatic inventory of road cross-sections from mobile laser scanning system," *Comput.-Aided Civil Infrastructure Eng.*, vol. 32, no. 1, pp. 3–17, 2017.
[40] Y. Zhou et al., "Highway alignments extraction and 3D modeling from airborne laser scanning point clouds," *Int. J. Appl. Earth Observ. Geoinformation*, vol. 102, 2021, Art. no. 102429.
[41] J. Antonio Martin-Jimenez et al., "Road safety evaluation through automatic extraction of road horizontal alignments from Mobile LiDAR System and inductive reasoning based on a decision tree," *ISPRS J. Photogrammetry Remote Sens.*, vol. 146, pp. 334–338, 2018.
[42] S. Oude Elberink and G. Vosselman, "3D information extraction from laser point clouds covering complex road junctions," *Photogrammetric Rec.*, vol. 24, pp. 23–36, 2009.
[43] F. Jiang et al., "Building digital twins of existing highways using map data based on engineering expertise," *Automat. Construction*, vol. 134, 2022, Art. no. 104081.
[44] H. Han et al., "An adaptive surface filter for airborne laser scanning point clouds by means of regularization and bending energy," *ISPRS J. Photogrammetry Remote Sens.*, vol. 92, no. 2, pp. 98–111, 2014.
[45] H. Edelsbrunner, D. Kirkpatrick, and R. Seidel, "On the shape of a set of points in the plane," *IEEE Trans. Inf. Theory*, vol. 29, no. 4, pp. 551–559, Jul. 1983.
[46] MTPRC, "Technical standard of highway engineering," Ministry of Transport of the People's Republic of China, 2004.
[47] H. Tveite and S. Langaas, "An accuracy assessment method for geographical line data sets based on buffering," *Int. J. Geographical Inf. Sci.*, vol. 13, no. 1, pp. 27–47, 1999.

Ruifeng Ma received the M.S. degree in photogrammetry and remote sensing in 2019 from Lanzhou Jiaotong University, Lanzhou, China, where he is currently working toward the Ph.D. degree in surveying and mapping.

Since 2020, he has been a Joint Training Doctoral Student with the Faculty of Geosciences and Engineering, Southwest Jiaotong University, Chengdu, China. His research interests include photogrammetry, inverse 3D modeling of highway scenes, and mobile measure laser point clouds semantic segmentation.

Qing Zhu received the Ph.D. degree in railway engineering from Northern Jiaotong University, Beijing, China.

From 1995 to 1997, he was a Postdoctoral Fellow with Wuhan University, Wuhan, China. From 1998 to 2013, he was a Professor with the State Key Laboratory of Information Engineering in Surveying, Mapping, and Remote Sensing, Wuhan University. He is currently a Professor with the Faculty of Geosciences and Engineering, Southwest Jiaotong University, Chengdu, China. His research interests include the digital elevation model, 3-D GIS, virtual geographic environments, and smart city.

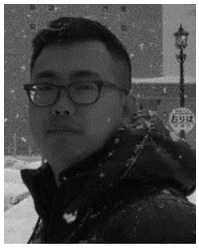

Xuming Ge received the Ph.D. degree in geodesy from the Technical University of Munich, Munich, Germany, in 2016.

From 2017 to 2019, he was a Postdoctoral Fellow with the Department of Land Surveying and Geo-Informatics, The Hong Kong Polytechnic University. He is currently a Professor with the Faculty of Geosciences and Engineering, Southwest Jiaotong University, Chengdu, China. His research interests include photogrammetry, 3D reconstruction, point cloud processing, and sensors calibration.

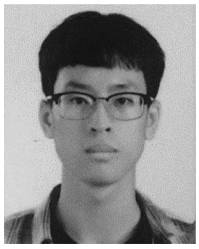

Xin Jia received the B.S. degree in cartography and geography information systems in 2020 from Lanzhou Jiaotong University, Lanzhou, China, where he is currently working toward the Ph.D. degree in surveying and mapping.

Since 2020, he has been a Joint Training Doctoral Student with the Faculty of Geosciences and Engineering, Southwest Jiaotong University, Chengdu, China. His research interests include point cloud processing and 3D reconstruction.

Han Hu (Member, IEEE) received the B.S. and Ph.D. degrees in photogrammetry and remote sensing from Wuhan University, Wuhan, China, in 2010 and 2015, respectively.

From 2015 to 2019, he was a Postdoctoral Fellow with The Hong Kong Polytechnic University, Hong Kong. He is currently a Professor with the Faculty of Geosciences and Engineering, Southwest Jiaotong University, Chengdu, China. His research interests focus on 3-D reconstruction of our planet Earth globally and regionally using datasets collected from satellites, aircraft, drones, vehicles, backpacks, and handheld devices.

Tao Liu received the B.S. and Ph.D. degrees in cartography and geographic information engineering from Wuhan University, Wuhan, China, in 2003 and 2011, respectively.

He is currently a Professor with the Faculty of Geomatics, Lanzhou Jiaotong University, Lanzhou, China. His research interests include spatial relationship theory, integration of GIS and remote sensing, and application and development of GIS and RS.